of the spacecraft, and we can infer that the negative space charge concentration on that side of the spacecraft leads to a local potential on the order of 500 mV relative to the spacecraft.

This being the case, a criterion for vanishing deflection of the particles is that they have energies of greater than about 10 times the value of 500 meV. Thus, 5-eV and higher-energy particles are relatively unaffected by the disturbed sheath, except that they do, of course, lose (or gain) about 2 eV of energy upon approach to the spacecraft in the case of the ions (or the electrons). Clearly, we have no reason to expect that the high-Mach-number ion flows observed by the TIDE should be significantly deflected by the PSI sheath disturbance. On the other hand, the ambient electrons accompanying these ion flows have much smaller flow energy, larger thermal velocity, and lower Mach number. Clearly, the core electrons below 5 eV (~7-eV measured energy) should exhibit detectable effects of deflection in these disturbed sheath fields. Subtle departures from electron gyrotropy may be observed at somewhat higher energies as well. These values can be used to interpret the observations from the TIDE as well as other instruments and to guide numerical model development to gain a quantitative understanding of the details of the potential structure. This model can in turn be used to develop empirical expressions to compensate for the effects of the PSI on observations of the natural environment.

Conclusions

Observations clearly demonstrate that the PSI has had the desired effect on the TIDE measurements: Low-energy ions that would otherwise be unobservable are seen. Equally clear is that the PSI modifies the sheath structure around the POLAR spacecraft in ways that also affect measurements made by other instruments, such as the PWI and the EFI. This implies that it will also have quantitative consequences for the TIDE observations. The EFI observations suggest that the TIDE core ion measurements will not be significantly affected unless ion energies are much less than 5 eV. Core electrons are more affected by the PSI sheath, and at lower outflow speeds the ions will also be influenced, requiring a better understanding of the sheath. A physical model has been presented that explains qualitatively the origin of the anisotropy found in observations with the PSI operating. This model can be used to guide the development of a detailed and accurate numerical model, which in turn can be used to develop modifications to the analysis to compensate for the PSI effects. The best understanding of the PSI sheath will come from synoptic operations of the PSI and dedicated analysis of the complete POLAR plasma data set.

Acknowledgment

The work done by R. H. Comfort was supported by NASA Grant NCC8-65 to the University of Alabama in Huntsville.

References

[1]Williams, J. D., and Wilbur, P. J., "Experimental Study of Plasma Contactor Phenomena," *Journal of Spacecraft and Rockets*, Vol. 27, No. 6, 1990, pp. 634–641.

[2]Ferguson, D. C., and Hillard, G. B., "In-Space Measurement of Electron Current Collection by Space Station Solar Arrays," AIAA Paper 95-0486, Jan. 1995.

[3]Chaky, R. C., and Lambert, J. C., "The ISS Plasma Contactor," AIAA Paper 96-0627, Jan. 1996.

[4]Patterson, M. J., Verhey, T. R., Soulas, G., and Zakany, J., "Space Station Cathode Design, Performance, and Operating Specifications," 25th International Electric Propulsion Conf., IEPC Paper 97-170, Cleveland, OH, Aug. 1997.

[5]Schmidt, R., Arends, H., Pedersen, A., Rudenauer, F., Fehringer, M., Narheim, B. T., Svenes, R., Kvernsveen, K., Tsuruda, K., Mukai, T., Hayakawa, H., and Nakamura, M., "Results from Active Spacecraft Potential Control on the Geotail Spacecraft," *Journal of Geophysical Research*, Vol. 100, No. A9, 1995, pp. 17,253–17,259.

[6]Acuna, M. H., Ogilvie, K. W., Baker, D. N., Curtis, S. A., Fairfield, D. H., and Mish, W. H., "The Global Geospace Science Program and Its Investigations," *Space Science Reviews*, Vol. 71, 1995, pp. 5–21.

[7]Moore, T. E., Chappell, C. R., Chandler, M. O., Fields, S. A., Pollock, C. J., Reasoner, D. L., Young, D. T., Burch, J. L., Eaker, N., Waite, J. H., Jr., McComas, D. J., Nordholdt, J. E., Thomsen, M. F., Berthelier, J. J., and Robson, R., "The Thermal Ion Dynamics Experiment and Plasma Source Instrument," *Space Science Reviews*, Vol. 71, 1995, pp. 409–458.

[8]Harvey, P., Mozer, F. S., Pankow, D., Wygant, J., Maynard, N. C., Singer, H., Sullivan, W., Anderson, P. B., Pfaff, R., Aggson, T., Pedersen, A., Falthammar, C.-G., and Tanskannen, P., "The Electric Field Instrument on the Polar Satellite," *Space Science Reviews*, Vol. 71, 1995, pp. 583–596.

[9]Gurnett, D. A., Persoon, A. M., Randall, R. F., Odem, D. L., Remington, S. L., Averkamp, T. F., Debower, M. M., Hospodarsky, G. B., Huff, R. L., Kirchner, D. L., Mitchell, M. A., Pham, B. T., Phillips, J. R., Schintler, W. J., Sheyko, P., and Tomash, D. R., "The Polar Plasma Wave Instrument," *Space Science Reviews*, Vol. 71, 1995, pp. 597–622.

[10]Su, Y.-J., Horwitz, J. L., Moore, T. E., Chandler, M. O., Craven, P. D., Giles, B. L., Hirahara, M., and Pollock, C. J., "Polar Wind Survey with TIDE/PSI Suite Aboard POLAR," *Journal of Geophysical Research* (to be published).

[11]Leung, W. C., Singh, N., and Moore, T. E., "Numerical Model of the Plasma Sheath Generated by the Plasma Source Instrument Aboard the Satellite in the Magnetosphere," 1998 Spring Meeting of the American Geophysical Union, Paper SA22A-06, Boston, MA, May 1998; also *EOS, Transactions, American Geophysical Union*, Vol. 79, April 1998, p. S234.

A. C. Tribble
Associate Editor

Computational Prediction of Pitch Damping for Supersonic Blunt Cones

D. K. Ludlow* and N. Qin†
Cranfield College of Aeronautics, Cranfield, Bedfordshire, England MK43 0AL, United Kingdom

Nomenclature

C_m, C_n	= pitching and side moment coefficients, respectively, (moment)/$\frac{1}{8}\pi\rho V^2 D^3$
C_{m_q}, $C_{m_{\dot\alpha}}$	= individual pitch damping coefficients: the rate of change of C_m with q and $\dot\alpha$, respectively
$C_{m_q} + C_{m_{\dot\alpha}}$	= pitch damping coefficient sum
C_p	= pressure coefficient, (pressure)/$\frac{1}{2}\rho V^2 - 2/(\gamma M^2)$
D	= projectile diameter, m
M	= freestream Mach number
p	= spin rate of body nondimensionalized by $2V/D$
q	= transverse angular velocity of body nondimensionalized by $2V/D$
Re	= Reynolds number based on D
T	= freestream temperature, K
V	= freestream velocity, m/s
x	= coordinate distance from (blunt) nose tip along body's longitudinal axis in D
x_{cg}	= axial location of center of gravity of body from (blunt) nose tip in D
α	= angle of attack, deg
$\dot\alpha$	= rate of change of α with respect to time nondimensionalized by $2V/D$
β	= side slip angle, deg
γ	= gas constant for air (1.4)
ρ	= freestream density, kg/m^3
Ω	= angular rate of noninertial coordinate frame about inertial frame, nondimensionalized by $2V/D$

Presented as Paper 98-0394 at the AIAA 36th Aerospace Sciences Meeting, Reno, NV, Jan. 12–15, 1998; received March 27, 1998; revision received Aug. 15, 1998; accepted for publication Sept. 10, 1998.

*Research Officer, Flow Control and Prediction Group.

†Senior Lecturer, Flow Control and Prediction Group. Senior Member AIAA.

Introduction

METHODS to predict pitch-damping coefficients (PDCs) of bodies from steady flow computations, avoiding costly time-accurate solutions, have been proposed by Schiff.[1,2] Lunar coning motion is imposed on the projectile, and the flow governing equations are solved in the rotating framework for which the flow is steady. Coning motion is the motion performed by an object flying at a constant angle of attack with respect to the freestream velocity vector and undergoing rotation at a constant angular velocity about a line parallel to the freestream flow direction passing through the projectile's c.g. Use of a moment expansion[3,4] then allows prediction of the PDC sum ($C_{m_q} + C_{m_{\dot\alpha}}$) from static moment coefficients in the frame of reference for which the flow is steady. Experimental measurements performed by Schiff and Tobak[5] provided additional support for this theory. Previously, much of these aerodynamic data was obtained from either simplified analytical approaches, empirical methods, wind-tunnel testing, or full-scale range firings.

In the preceding lunar coning approach, the Magnus moment coefficient was neglected. Although this assumption is supported by experimental evidence in some cases, Magnus effects may be important. Weinacht et al.,[6] however, showed that, for axisymmetric bodies undergoing $p = 0$ coning motion, the moment expansion no longer depends on Magnus effects. In $p = 0$ coning motion, the projectile has no spin about its longitudinal axis with respect to the inertial frame.

It is difficult to extract individual PDCs $C_{m_{\dot\alpha}}$ and C_{m_q} from free-flight aerodynamic ranges. Weinacht,[7] however, extended the use of imposed motions in a rotating framework to allow the determination of individual components of the PDC sum. This can be done by considering two different motions where the axisymmetric projectile's c.g. traverses a helical flight path: 1) steady $p = q = 0$ helical motion, where the body's longitudinal axis is parallel to the axis of the helix, and 2) $\dot\alpha = 0$ helical motion, where the body's longitudinal axis is tangent to its flight path.

Schiff[1,2] modeled the resulting steady flow with noninertial space-marching Euler equations, whereas more recently, the noninertial parabolized Navier–Stokes (PNS) have been used by several authors, e.g., Refs. 6–11. If, however, there is a region of flow outside the boundary layer that is not supersonic in the positive streamwise direction, the parabolic assumptions are no longer valid. One such example considered here are blunt-nosed bodies, for which a full three-dimensional Navier–Stokes (NS) methodology is presented. Concurrently, Weinacht[12] has used a three-dimensional NS methodology to predict PDCs for subsonic and transonic projectiles. A three-dimensional NS methodology may in the future enable prediction of the contribution to the PDCs due to the projectile's base.

Numerical Method and Results

The governing equations are the three-dimensional NS equations in a noninertial framework in which coning and helical motions can be implemented. The present numerical method employed solves the three-dimensional NS equations using a high-resolution finite volume scheme. Inviscid fluxes are evaluated using Osher's approximate Riemann solver together with third-order MUSCL interpolation of the flow primitive variables and a van Albada flux limiter. The diffusive terms in the governing equations were evaluated using second-order central differences, and any turbulence was accounted for by the Baldwin–Lomax algebraic model with the Degani–Schiff modification. Convergence to the steady-state solution is obtained by starting from freestream conditions and performing explicit local time marching until the steady solution is reached. To accelerate convergence, a zonal approach has also been used, where the CPU time-consuming, three-dimensional NS solution is used only to determine the flowfield in the subsonic nose region. Downstream from this region a PNS solver[11] has been initialized to solve the flowfield. More details of the numerical method can be found in Ref. 13.

Initially, to validate the three-dimensional NS method, we recalculated the cone–cylinder–flare geometry under high-Mach-number flow conditions with turbulent boundary layer as studied in Ref. 11 by the PNS technique. The results obtained with the present methodology were, as expected, graphically identical to those of the earlier PNS work and are not shown here.

The blunt projectile under consideration is a 10-deg half-angle cone of base diameter D with the pointed nose replaced by a circular arc of diameter $0.3D$ such that the arc and the cone are tangential where they meet. Unless stated otherwise, $x_{cg} = 1.21$, $M = 6.85$, $Re = 1.79 \times 10^6$, $T = 58$ K, the wall temperature is fixed at 288 K, and pressure at the wall is assumed to have zero gradient normal to the wall. Some PDC sum data for such a geometry and laminar flow conditions have been published by East et al.,[14] Khalid and East,[15] and Tong and Hui[16] using wind-tunnel experiments, semiempirical, and theoretical methods.

Unless stated otherwise, the computations were performed on a single grid with 32 cells in each direction. The grid is axisymmetric about the cone's axis and is stretched toward the projectile's surface and nose to fully resolve the boundary layer, geometry, and high-pressure gradients. The base-flow region is not modeled. As part of the validation procedure, in Fig. 1 we show that, for coning motion, the calculated side moment is, as required, a linear function of both α and Ω in a region about the origin. A slight irregularity for $\alpha = 0.5$ deg may be due to increased numerical errors for such a small α. In the following calculations, the PDCs are determined using imposed coning and helical motions with α (or β) equal to 1 deg and $\Omega = 0.00225$. To gauge the convergence of the scheme, the base 10 logarithm of the Euclidean norm of the residual vector normalized by its freestream value is monitored together with the predicted PDC every 10 iterations. A typical convergence history, shown in Fig. 2, shows that the PDC value has converged to a stable value with six orders of convergence of the residual.

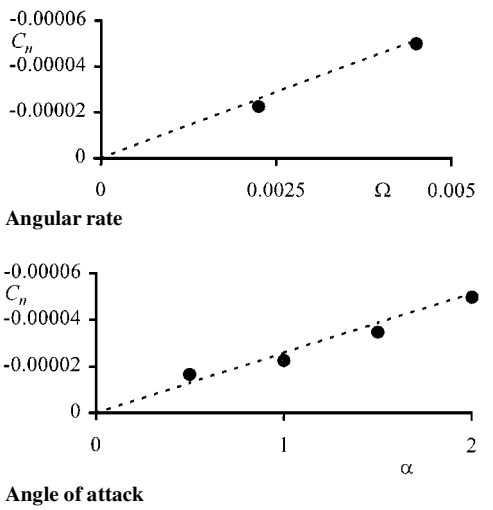

Fig. 1 Variation of side moment with α and Ω for $p = 0$ coning motion.

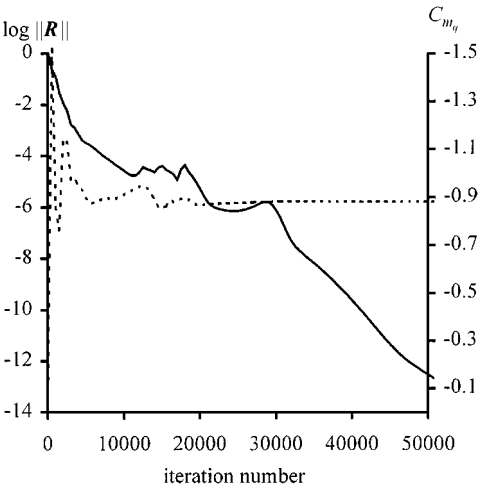

Fig. 2 Typical convergence history: ——, residual, and - - - -, PDC for $\dot\alpha = 0$ helical motion.

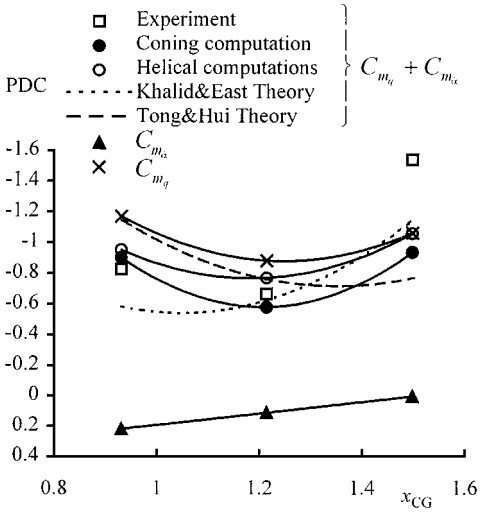

Fig. 3 Evaluated PDCs from imposed motions.

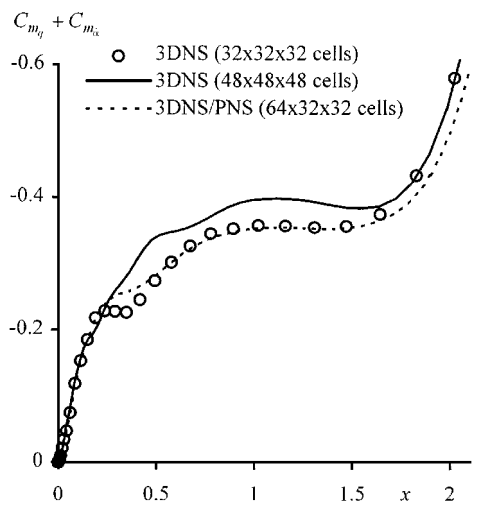

Fig. 4 Cumulative PDC sum for generic $p = 0$ coning motion.

In Fig. 3, the PDCs obtained by the present computational method using coning and both helical motions are plotted for three different c.g. positions together with experimental results obtained in Ref. 14 and semiempirical/theoretical methods presented in Refs. 15 and 16. There is reasonable agreement between experiment and both computations for the first two c.g. positions (from left to right); however, there is a large discrepancy for the third case. The results of the two theoretical models plotted in Fig. 3, however, also fail to produce a PDC as large as the experiment. The reason behind this discrepancy is unclear and requires further investigation, but generally the computed data give better comparison with the experimental data than either theoretical model. There do not appear to be any experimental data to compare the results obtained from either of the helical motions; however, in Fig. 3, we show that the sum of the evaluated individual PDCs is in reasonable agreement with the data from the coning motion. For the present case, the viscous contributions to the PDC sum is small as compared with the inviscid one, typically two orders smaller. However, for the individual PDC $C_{m_{\dot\alpha}}$, the viscous contribution can be significant, justifying inclusion of viscous terms.

The issues of grid convergence and use of the zonal method are addressed in Fig. 4, which shows the contribution to the PDC from each grid slice in the streamwise direction by the sum of the contribution to the PDC from the present grid slice with all of the upwind grid slices for three different calculations. The evaluated projectile PDC is then just the farthest-right point of each graph line. The fine grid ($48 \times 48 \times 48$) is seen in Fig. 4 to produce a result closer to the experimental data than the coarser grid ($32 \times 32 \times 32$), but the overall difference is small, and so the results obtained on the coarser grid are considered reasonable for a reasonable amount of computational effort. The $32 \times 32 \times 32$ mesh, however, was found to be not adequate to obtain good agreement between the full three-dimensional NS approach and the zonal approach. For the two approaches to give reasonable agreement, it was necessary to increase the number of cells in the streamwise direction for the PNS part of the calculation because the PNS calculation is only first order in the streamwise spatial direction compared with the higher-order three-dimensional NS approach. A calculation using the zonal approach is also shown in Fig. 4; here the three-dimensional NS equations have been solved on the first 16 cell planes of the $32 \times 32 \times 32$ computational mesh. The second half of the grid has been refined in the streamwise direction before solution of the PNS equations; the resulting grid consists of a total of $64 \times 32 \times 32$ cells. The PDC profile is shown in Fig. 4 to be close to the three-dimensional NS approach. Despite the addition of extra cells, the CPU time required for the PNS part of the zonal approach is still negligible compared with the time required for the three-dimensional NS part. Hence, the zonal approach is approximately two times faster.

Acknowledgments

This research was partially supported by the U.K. Defence and Evaluation Research Agency (DERA). The authors would like to thank Scott Shaw of Cranfield College of Aeronautics and John Edwards of DERA for helpful discussions.

References

[1]Schiff, L. B., "A Study of the Nonlinear Aerodynamics of Bodies in Non-Planar Motion," NASA TR-R-421, Jan. 1974.

[2]Schiff, L. B., "Nonlinear Aerodynamics of Bodies in Coning Motion," *AIAA Journal*, Vol. 10, No. 11, 1972, pp. 1517–1522.

[3]Murphy, C. H., "Free Flight Motion of Symmetric Missiles," U. S. Army Ballistic Research Lab., Rept. 1216, Aberdeen Proving Ground, MD, July 1963.

[4]Tobak, M., Schiff, L. B., and Peterson, V. L., "Aerodynamics of Bodies of Revolution in Coning Motion," *AIAA Journal*, Vol. 7, No. 1, 1969, pp. 95–99.

[5]Schiff, L. B., and Tobak, M., "Results from a New Wind-Tunnel Apparatus for Studying Coning and Spinning Motions of Bodies of Revolution," *AIAA Journal*, Vol. 8, No. 11, 1970, pp. 1953–1957.

[6]Weinacht, P., Sturek, W. B., and Schiff, L. B., "Navier–Stokes Predictions of Pitch Damping for Axisymmetric Shell Using Steady Coning Motion," AIAA Paper 91-2855, Aug. 1991.

[7]Weinacht, P., "Navier–Stokes Predictions of the Individual Components of the Pitch-Damping Coefficient Sum," AIAA Paper 95-3485, Aug. 1995.

[8]Agarwal, R., and Rakich, J. V., "Computation of Supersonic Laminar Viscous Flow Past a Pointed Cone at Angle of Attack in Spinning and Coning Motion," AIAA Paper 78-1211, July 1978.

[9]Lin, T. C., "A Numerical Study of the Aerodynamics of a Re-Entry Vehicle in Steady Coning Motion," AIAA Paper 78-1358, Aug. 1978.

[10]Weinacht, P., and Sturek, W. B., "Navier–Stokes Prediction of Static and Dynamic Aerodynamic Derivatives for High L/D Finned Projectiles," *Missile Aerodynamics*, CP-493, AGARD, 1990, pp. 20.1–20.12.

[11]Qin, N., Ludlow, D. K., Shaw, S. T., Edwards, J. A., and Dupuis, A., "Calculation of Pitch Damping for a Flared Projectile," *Journal of Spacecraft and Rockets*, Vol. 34, No. 4, 1997, pp. 566–568.

[12]Weinacht, P., "Prediction of Pitch-Damping of Projectiles at Low Supersonic and Transonic Velocities," AIAA Paper 98-0395, Jan. 1998.

[13]Ludlow, D. K., and Qin, N., "Computational Prediction of Pitch Damping for High Mach Number Blunt Projectiles," AIAA Paper 98-0394, Jan. 1998.

[14]East, R. A., Qasrawi, A. M. S., and Khalid, M., "An Experimental Study of the Hypersonic Dynamic Stability of Pitching Blunt Conical and Hyperballistic Shapes in a Short Running Time Facility," *Dynamic Stability Parameters*, CP-235, AGARD, 1978, pp. 12.1–12.20.

[15]Khalid, M., and East, R. A., "Stability Derivatives of Blunt Slender Cones at High Mach Numbers," *Aeronautical Quarterly*, Vol. 30, Nov. 1979, pp. 559–589.

[16]Tong, B.-G., and Hui, W. H., "Unsteady Embedded Newton–Busemann Flow Theory," *Journal of Spacecraft and Rockets*, Vol. 23, No. 2, 1986, pp. 129–135.

R. M. Cummings
Associate Editor